Capacity of Polarized-MIMO (P-MIMO) System in Different Wireless Channels

Seungcheol Paul Oh and Seok-Chul Sean Kwon
Department of Electrical Engineering, California State University Long Beach
Email: seungcheol.oh@student.csulb.edu, sean.kwon@csulb.edu

***Abstract*—The channel capacity of multiple input multiple output (MIMO) wireless communication systems can be remarkably improved via using polarization diversity. It is obvious that the aforementioned improvement can save transmission power/energy; therefore, contribute to green communications. Recent researches have proposed system designs to utilize antennas with multiple polarization. A MIMO communication system that utilizes these antennas will improve its channel capacity if optimal polarization vectors are used. This paper provides analysis and evaluation of the improvement in channel capacity for different wireless channels via employing the polarized-MIMO (P-MIMO) system. Comprehensive simulation results are provided to show that P-MIMO system can substantially improve channel capacity in additive white Gaussian noise (AWGN), Rayleigh, and Rician fading channels. These three channel distributions are used in the simulations to observe the effect that each has on the P-MIMO system. Each channel exhibits different characteristics from other channels.**

I. Introduction

The utilization of polarization diversity and the employment of polarized multiple input multiple output (P-MIMO) scheme in wireless communication systems can significantly increase the system's channel sum capacity [1]–[6]. However, latest researches tend to have utilized dual-polarized antennas for polarization diversity. In the aforementioned scenario, polarization of both the transmitter and receiver is, generally, fixed in the communication system. This scenario causes mismatch between the optimal polarization of the Tx/Rx; and the practical random polarization of small hand-held wireless devices, which results in the loss of channel capacity. To compensate for the loss, polarization-agile antennas have been suggested by the recent research [7], [8]. The loss of channel capacity can be remarkably mitigated with polarization-agile antennas. The polarization-agile antenna not only includes vertical and horizontal polarization components but has additional 45° and 135° in between. That is, the polarization-agile antenna can provide further polarization components, and ultimately, is expected to yield much smaller granularity than 45° or continuous polarization components in the future.

The multiple input multiple output (MIMO) communication system can adopt the polarization-agile antenna elements, i.e., P-MIMO communication system, such that its channel capacity will increase, and further, its bit error rate will decrease. The aforementioned MIMO system with polarization-agile antenna elements is called "polarized-MIMO" (P-MIMO) [9]. The contributions of this paper can be summarized as listed:

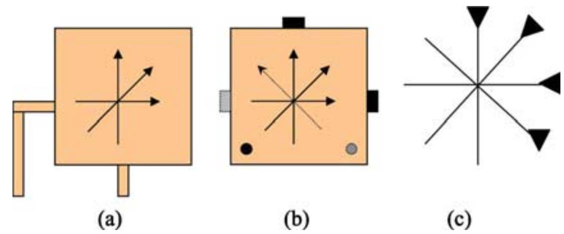

Fig. 1. Polarization-agile antenna.

- analysis of the improvement in channel capacity via adopting P-MIMO system based on simulation;
- simulation results validating satisfactory improvement in channel capacity for three different scenarios of wireless channels;
- simulation results that compare P-MIMO system's channel capacity with varying SNR and varying number of polarization-agile antenna elements in three different channel scenarios;
- observation on the effect that three different channel distributions, i.e., AWGN, Rayleigh, and Rician, have on the P-MIMO system.

The remainder of this paper is organized as follows. Section II describes how polarization-agile antennas function; Section III describes the MIMO system with polarization-agile antennas and provides mathematical derivations on finding the optimal polarization vectors, and Section IV compares numerical and theoretical results with three different channels. Lastly, Section V concludes the paper.

II. Polarization-agile Antenna

According to [7], numerous researchers have only exploited dual-polarized antennas in their scenarios of wireless communications; this means that the scenarios only consist of either 0° or 90° polarization. Such a case is ineffective because in a practical sense, cell phones are subjected to have polarization mismatch losses due to its polarization not always being 0° or 90°. Hence, further polarization components have to be implemented in wireless communication systems to counter the polarization mismatch losses. Thus, an inexpensive way to design such antennas is offered by [7]. Figure 1 displays three antennas. Figure 1(a) is the dual-polarized antenna which can only transmit and receive 0° and 90° linear polarization. This antenna has two feed ports and depending on which port is turned on, the degree of the polarization is transmitted or received. Figure 1(b) has a single feed(black dot) and two positive intrinsic negative diodes(black rectangles). The purpose for two diodes is to switch between 0°, 45°, or 90° polarization. For the 135° to work, second feed point, in gray, has to turn on. Figure 1(c) weep out linear polarization of 0°, 45°, 90°, and 135°. These antennas with multiple polarization elements are referred as polarization-agile antennas. More polarization elements can be implemented in antennas until the point it reaches continuous polarization [8]. This antenna with continuous polarization elements is used in P-MIMO communication system.

III. Polarized-MIMO (P-MIMO) System

The system model that uses polarization-agile antennas in MIMO communication system is shown in Fig. 2. The system is MIMO, which implies that it has multiple antenna elements at both transmitter (Tx) and receiver (Rx) sides. As shown, each antenna element has continuous polarization. With polarization-agile antennas and pre-post coding based on singular value decomposition, the system can reach higher capacity than a system that uses random polarization or dual-polarization. The mathematical derivation to prove this will be shown below.

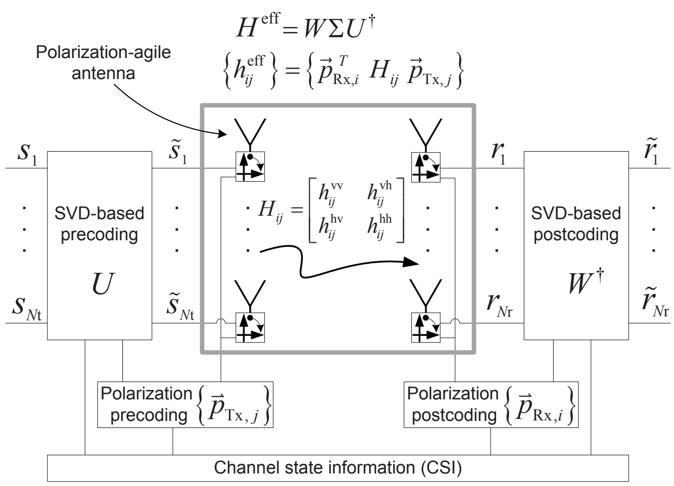

Fig. 2. MIMO system with polarization-agile antenna.

The effective channel impulse response, H^{eff}, of P-MIMO system is represented as

$$H^{\text{eff}} = \begin{bmatrix} \vec{p}_{\text{Rx},1}^{\,T} H_{11} \vec{p}_{\text{Tx},1} & \dots & \vec{p}_{\text{Rx},1}^{\,T} H_{1N_{\text{t}}} \vec{p}_{\text{Tx},N_{\text{t}}} \\ \vdots & \ddots & \vdots \\ \vec{p}_{\text{Rx},N_{\text{r}}}^{\,T} H_{N_{\text{r}}1} \vec{p}_{\text{Tx},1} & \dots & \vec{p}_{\text{Rx},N_{\text{r}}}^{\,T} H_{N_{\text{r}}N_{\text{t}}} \vec{p}_{\text{Tx},N_{\text{t}}} \end{bmatrix}, \tag{1}$$

in which $(\cdot)^T$ means transpose of a matrix or vector. The dimension of H^{eff} is determined by $N_{\text{r}} \times N_{\text{t}}$. Furthermore, H_{ij} is "polarization-basis matrix" which is characterized below as

$$H_{ij} = \begin{bmatrix} h_{ij}^{\text{vv}} & h_{ij}^{\text{vh}} \\ h_{ij}^{\text{hv}} & h_{ij}^{\text{hh}} \end{bmatrix}, \tag{2}$$

where h_{ij}^{xy} is the XY-channel impulse response with $\text{x} \in \{\text{v}, \text{h}\}$; $\text{y} \in \{\text{v}, \text{h}\}$. Finally, $\vec{p}_{\text{Tx},j}$ and $\vec{p}_{\text{Rx},i}$ are polarization vectors expressed as,

$$\vec{p}_{\text{Tx},j} = \begin{bmatrix} p_{\text{Tx},j}^{\text{v}} \\ p_{\text{Tx},j}^{\text{h}} \end{bmatrix} = \begin{bmatrix} \cos\theta_j \\ \sin\theta_j \end{bmatrix}, \tag{3}$$

$$\vec{p}_{\text{Rx},i} = \begin{bmatrix} p_{\text{Rx},i}^{\text{v}} \\ p_{\text{Rx},i}^{\text{h}} \end{bmatrix} = \begin{bmatrix} \cos\theta_i \\ \sin\theta_i \end{bmatrix}. \tag{4}$$

The channel impulse response is decomposed by singular value decomposition (SVD) to find the polarization pre-post coding. When H^{eff} is decomposed with SVD, the equation is defined as

$$H^{\text{eff}} = W\Sigma U^{\dagger}, \tag{5}$$

where Σ is the diagonal matrix, and W and $U^{\dagger}$ are unitary matrices. In addition, $(\cdot)^{\dagger}$ represents conjugate transpose of a matrix (Hermitian transpose). With the SVD based pre-post coding, maximum channel capacity of the system is found to be

$$C = \sum_{k=1}^{R_{H^{\text{eff}}}} \log_2 \left(1 + \frac{P_k}{{\sigma_n}^2} {\sigma_k}^2\right), \tag{6}$$

where $R_{H^{\text{eff}}}$ is the rank of effective channel matrix. $\frac{P_k}{{\sigma_n}^2}{\sigma_k}^2$ is signal to noise power ratio. ${\sigma_n}^2$ is the noise power, P_k is the power allocated to the kth eigenmode. Lastly, ${\sigma_k}^2$ is kth value of the effective channel impulse response matrix. P_k is determined by water-filling power allocation,

$$P_k = \max\left(0, \epsilon - \frac{{\sigma_n}^2}{{\sigma_k}^2}\right) \text{ s.t. } P = \sum_{k=1}^{R_{H^{\text{eff}}}} P_k \ , \tag{7}$$

where ϵ is the threshold that is determined by the constraint of total transmitted power P. Using Jensen's inequality from [10],

$$C \leq R_{H^{\text{eff}}} \log_2 \left(1 + \frac{1}{R_{H^{\text{eff}}}} \sum_{k=1}^{R_{H^{\text{eff}}}} \frac{P_k}{{\sigma_n}^2} {\sigma_k}^2\right) \tag{8}$$

$$= R_{H^{\text{eff}}} \log_2 \left(\frac{1}{R_{H^{\text{eff}}}} \frac{\epsilon}{{\sigma_n}^2} \sum_{k=1}^{R_{H^{\text{eff}}}} {\sigma_k}^2\right) \tag{9}$$

is obtained. ${\sigma_k}^2$ is the eigen value of $\text{Tr}\big(H^{\text{eff}}(H^{\text{eff}})^{\dagger}\big)$ which yield,

$$\sum_{k=1}^{R_{H^{\text{eff}}}} {\sigma_k}^2 = \text{Tr}\left(H^{\text{eff}}(H^{\text{eff}})^{\dagger}\right) = \sum_{n,m} \left|h_{nm}^{\text{eff}}\right|^2. \tag{10}$$

Based on Linear Algebraic operations from [11], optimal transmit polarization vector $\vec{p}_{\text{Tx},j}^{\,\text{opt}}$ and optimal transmit polarization angle θ_j^{opt} are found. They are described as

$$\vec{p}_{\text{Tx},j}^{\,\text{opt}} = \arg\max_{\vec{p}_{\text{Tx},j}} \vec{p}_{\text{Tx},j}^{\,T} H_{\text{Tx},j}^{\text{PD}} \vec{p}_{\text{Tx},j} = \vec{e}_2, \tag{11}$$

$$\theta_j^{\text{opt}} = \arctan(\vec{e_2}), \tag{12}$$

where

$$H^{\mathrm{PD}}_{\mathrm{Tx},j} \triangleq \sum_{i=1}^{N_{\mathrm{r}}} H^{\dagger}_{ij} \vec{p}_{\mathrm{Rx},i} \vec{p}^{\,T}_{\mathrm{Rx},i} H_{ij} \ . \tag{13}$$

In a complementary manner to equations (11) and (13), optimal received polarization vector and angle are found.

$$\vec{p}^{\,\mathrm{opt}}_{\mathrm{Rx},i} = \arg\max_{\vec{p}_{\mathrm{Rx},i}} \vec{p}^{\,T}_{\mathrm{Rx},i} H^{\mathrm{PD}}_{\mathrm{Rx},i} \vec{p}_{\mathrm{Rx},i} = \vec{e}_2, \tag{14}$$

$$\theta^{\mathrm{opt}}_{i} = \arctan(\vec{e_2}), \tag{15}$$

where the "*Rx-polarization-determinant matrix*" for the ith Rx polarization-agile antenna, $H^{\mathrm{PD}}_{\mathrm{Rx},i}$, is defined as

$$H^{\mathrm{PD}}_{\mathrm{Rx},i} \triangleq \sum_{j=1}^{N_{\mathrm{t}}} H_{ij} \vec{p}_{\mathrm{Tx},j} \vec{p}^{\,T}_{\mathrm{Tx},j} H^{\dagger}_{ij} \ . \tag{16}$$

As shown in (16), $H^{\mathrm{PD}}_{\mathrm{Rx},i}$, the Rx-polarization-determinant matrix at ith Rx polarization-agile antenna rely on Tx-polarization vectors $\vec{p}_{\mathrm{Tx},j}$. Hence, system's performance will degrade when Tx- and Rx-polarization are mismatched. This is why joint polarization pre-post coding is introduced to maximize the system's performance by increasing the channel capacity. The joint polarization pre-post coding is done through iteration. In the kth iteration stage, $\vec{p}^{\,\mathrm{opt},(k-1)}_{\mathrm{Tx},j}$ is updated to $\vec{p}^{\,\mathrm{opt},(k)}_{\mathrm{Tx},j}$ based on $\vec{p}^{\,\mathrm{opt},(k-1)}_{\mathrm{Rx},i}$ according to (13) – (12). Then, in , $\vec{p}^{\,\mathrm{opt},(k-1)}_{\mathrm{Rx},i}$ is updated to $\vec{p}^{\,\mathrm{opt},(k)}_{\mathrm{Rx},i}$ based on the updated $\vec{p}^{\,\mathrm{opt},(k)}_{\mathrm{Tx},j}$ following (14) – (16).

IV. Experiments and Results

This section provides simulation results for the impact of the P-MIMO system on different channel models. The first simulation assumes a high SNR regime of 30 dB. Each of Figs. 3 – 5 depicts four cumulative distribution functions (CDF) of 2×2 P-MIMO system channel capacity, where each curve is the result of applying different scheme or method of searching the optimal Tx/Rx polarization.

One curve represents CDF of channel capacity based on the optimal polarization that is resulted from the brute-force numerical search. On the other hand, another curve is the CDF of channel capacity based on the optimal polarization determined by the joint polarization pre-post coding. Further, each figure illustrates the CDF curves based on random polarization; and the worst-case polarization in joint polarization pre-post coding. Three channel models are used for the simulation: additive white Gaussian noise (AWGN), Rayleigh, and Rician fading channels. They result in distinctive CDF curves from each other depending on the assumption of wireless channels. AWGN channel results maximum channel capacity that is greater than that of the results in the assuption of Rayleigh and Rician fading channels; however, notice that AWGN channel is not a practical one. Rayleigh and Rician fading channels are practical; however, it is obvious that they do not yield better channel capacity than AWGN channel. Notice that the difference between Rayleigh and Rician fading channels is that the former only includes none line-of-site (NLoS) components; while the latter accommodates NLoS components along with the line-of-site (LoS) components.

The CDF curves of channel capacity in AWGN channel is exhibited in Fig. 3. As depicted, probability of getting channel capacity greater than 18.58 bits/sec/Hz is 0.90 with optimal theoretically searched polarization. On the other side, probability of getting channel capacity greater than 20.41 bits/sec/Hz is 0.90 with numerically searched polarization. Hence, the difference between them is 1.83 bits/sec/Hz. The difference however, decreases as the probability gets lower. As an evidence, probability of receiving channel capacity greater than 20.92 bits/sec/Hz is 0.50 with theoretically searched polarization. Also, with same probability, numerically searched polarization yields channel capacity of 21.59 bits/sec/Hz. Thus, the total difference with 0.50 probability is 0.67 bits/sec/Hz. Notice that in AWGN channel, CDF curve with theoretical polarization has great distance from CDF curve with random polarization. This extracts the information that the polarization-agile antennas with optimal joint pre-post coding results much better performance than dual-polarized antennas.

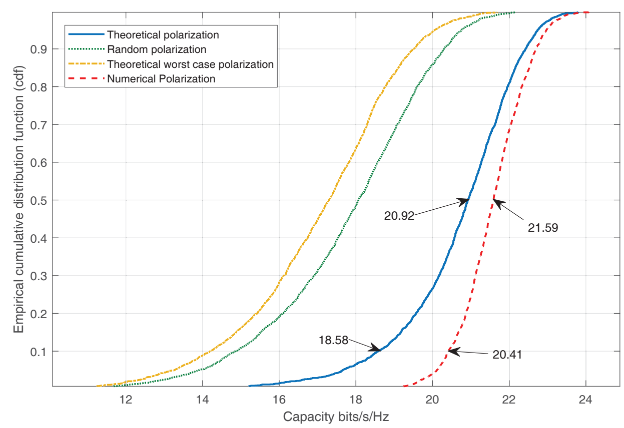

Fig. 3. Channel Capacity with AWGN Channel

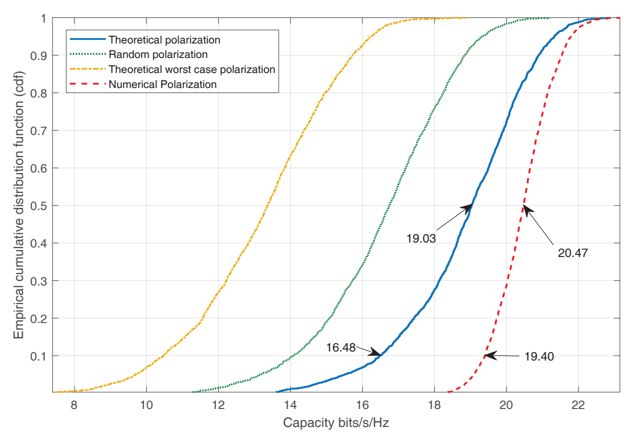

Fig. 4. Channel Capacity with Rayleigh Fading Channel

The CDF curves of channel capacity for Rayleigh fading channel is illustrated in Fig. 4. Note that Rayleigh fading

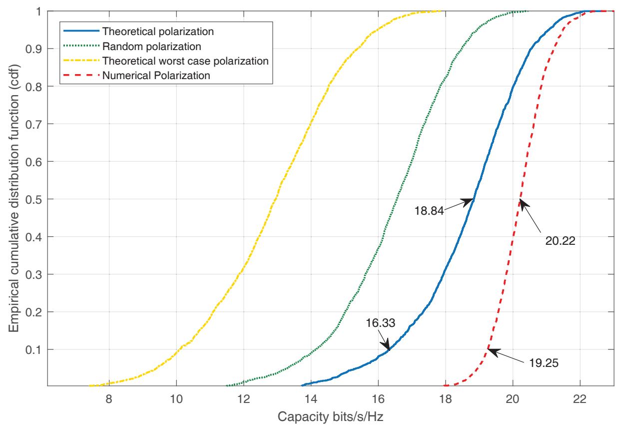

Fig. 5. Channel Capacity with Rician Fading Channel

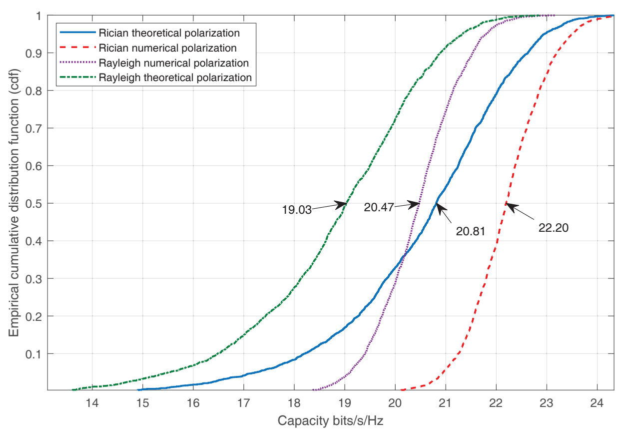

Fig. 6. Comparison Between Rayleigh and Rician Fading Channels

channel is a more practical channel than AWGN channel. Hence, it is obvious that all the CDF curves represent less channel capacity than that of the CDF curves of the AWGN channel. This is the reason why there is a more considerable difference between the CDF curves resulted from the theoretical approach and the numerical search. The probability of getting channel capacity greater than 16.48 bits/sec/Hz is 0.90 with theoretical polarization. Whereas with numerically found polarization with the same probability, channel capacity is 19.40 bits/sec/Hz. As with AWGN channel, the difference between the curves decreases as the cumulative probability increases in the scenario of Rayleigh fading channel. The probability of getting channel capacity greater than 19.03 bits/sec/Hz is 0.50 with theoretically found polarization and 20.47 bits/sec/Hz with numerically found polarization. As put on display, the channel capacity of each curves decreased in Rayleigh fading channel when compared to the curves with AWGN channel. In AWGN channel, difference between the numerical-search based and theoretical curves is equal to or greater than 1.83 bits/sec/Hz with the probability of 0.1; while in Rayleigh fading channel, the difference is equal to or greater than 2.92 bits/sec/Hz with the same probability. Moreover, correspondingly, the gap between CDF curves of random and theoretical polarization is less than that in AWGN channel.

The CDF curve of channel capacity in Rician fading channel is displayed in Fig. 5. Notice again that Rician fading channel includes both NLoS and LoS components; whereas, Rayleigh fading channel only includes line of site components. For that reason, CDF curves resulted from the assumption of Rician fading channel should be approximately shifted version of the results from the assumption of Rayleigh fading channel. It is worth mentioning, for the purpose of the evaluation, both LoS and NLoS components in the Rician fading channel were normalized. Therefore, even with the supplemented LoS components in a given channel, the CDF curves are not biased. As a proof, Fig. 5 closely relate with Fig. 4. As shown in Fig. 5 the probability of receiving a capacity greater than 16.33 bits/sec/Hz is 0.90 with theoretically obtained polarization. Whereas, with numerically searched polarization, it is 19.25 bits/sec/Hz; the difference between them is 2.82 bits/sec/Hz. Note that the difference is 2.92 bits/sec/Hz for Rayleigh, which means Rician and Rayleigh show similar results when they are both normalized.

The comparison of CDF curves in the scenarios of Rayleigh and Rician fading channels, is illustrated in Fig. 6. LoS components for Rician fading channel is not included in the normalization weight. The CDF curves for Rician fading channel should closely resemble ones for Rayleigh fading channel except the shift to the right in x-axis, which is caused by the NLoS components. This theoretical intuition is in a good agreement with Fig. 6.

In the next set of simulations, P-MIMO system's channel capacity for varying SNR from 0 dB to 30 dB and the varying number of polarization-agile antenna elements, 2×2 and 4×4, is provided, depending on different assumption of wireless channels, i.e., AWGN, Rayleigh, and Rician fading channels. For each scenario of the number of antenna elements, three curves were illustrated. The curves represent three scenarios: channel capacity resulted from random Tx and Rx polarization; only Tx polarization precoding at transmitter side; joint polarization pre-post coding at both Tx and Rx sides.

Channel capacity in AWGN channel with varying SNR and varying polarization-agile antenna components is shown in Fig. 7. As displayed, with high SNR regime, P-MIMO system greatly increases the system's capacity. Moreover, as the polarization-agile antenna elements increase from 2×2 to 4×4, the channel capacity significantly increased. With SNR regime of 27 dB, joint polarization pre-post coding yields 18.74 bits/sec/Hz, when the system is 2×2. Further, with the same SNR regime, joint polarization pre-post coding outcome 35.27 bits/sec/Hz in 4×4 system.

The same experiment was simulated in Rayleigh fading channel. The result of this is exhibited in Fig. 8. Similar to previous set of experiment, P-MIMO system in Rayleigh fading channel does not show better performance than the AWGN fading channel. As the figure shows, in the high SNR regime of 27 dB, channel capacity found with joint polarization pre-post coding is 28.88 bits/sec/Hz in 4×4

system. This displays that AWGN yield channel capacity that is nearly 1.2 times greater than the channel capacity found in Rayleigh channel when in 4×4 system.

The final simulation is ran in Rician fading channel. Rician fading channel is similar to Rayleigh fading channel except that it includes line of site components to its channel. Therefore, the result should have somewhat better results than the results of Rayleigh fading channel but not better than the results of AWGN. As exhibited, the channel capacity at 27 dB in 4×4 system is 31.85 bits/sec/Hz with joint polarization pre-post coding. As expected, the result is better than results drawn by Rayleigh channel but not better than AWGN channel. Note that in 2×2 system, channel capacity in Rician channel with joint pre-post coding polarization is not so much different than that is found in AWGN channel. In Rician, capacity is 18.61 bit/sec/Hz, while in AWGN, it is 18.74 bit/sec/Hz. However, in 4×4 system, the difference is greater: 31.85 bits/sec/Hz in Rician and 35.27 bits/sec/Hz in AWGN. That is because in AWGN channel, correlation between antenna elements are nearly zero; whereas in Rician channel, line of site components create correlation between the antenna elements. In 2×2 system, there are only 2 antenna elements; therefore, there is less correlation which is the reason why there is less difference. In 4×4 system, there is more correlation in Rician channel because of more antenna elements.

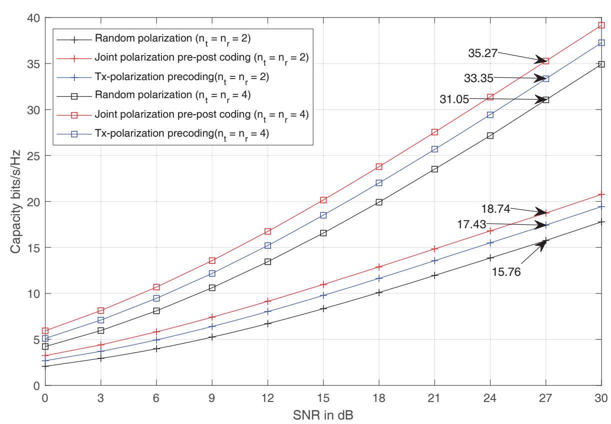

Fig. 7. P-MIMO channel capacity with varying SNR and polarization-agile antenna elements in AWGN fading channel

V. Conclusion

This paper provides comprehensive evaluation of the P-MIMO system, where the conventional MIMO system adopts polarization-agile antenna elements at both Tx and Rx. Three different assumptions on wireless channel condition were considered, i.e., AWGN, Rayleigh, and Rician fading channels. It is shown that the employment of polarization-agile antenna elements in MIMO communication systems significantly increases channel capacity for all the aforementioned wireless channels. The optimal polarization vectors and angles can be adjusted based on the theoretical approach with satisfactory performance comparing with the numerically searched polarization in all those three channels. AWGN channel exhibited

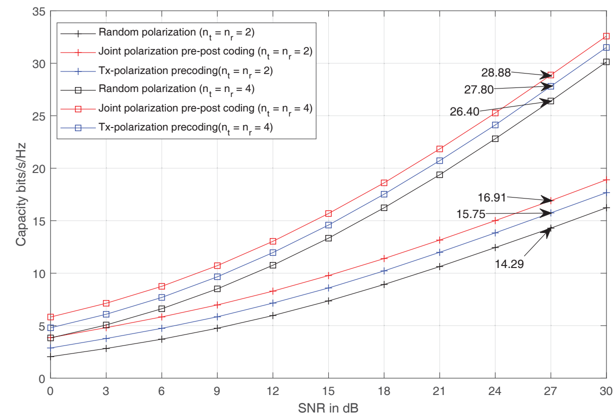

Fig. 8. P-MIMO channel capacity with varying SNR and polarization-agile antenna elements in Rayleigh fading channel

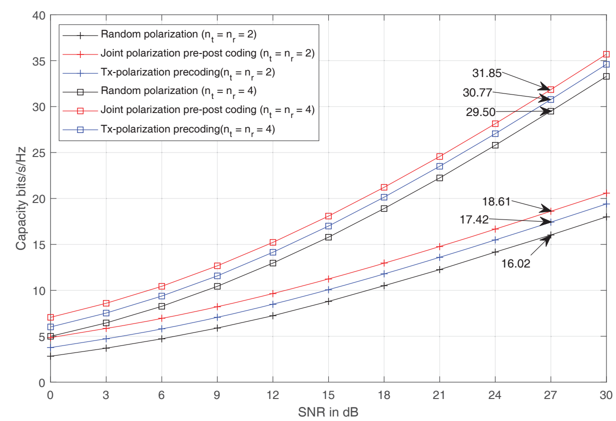

Fig. 9. P-MIMO channel capacity with varying SNR and polarization-agile antenna elements in Rician fading channel

the best improvement in channel capacity; on the other hand, the scenarios of Rayleigh and Rician fading channels has potential in that channel capacity resulted from the theoretical approach can be more improved. This will be our future research work.

References

[1] R. G. Vaughan, "Polarization diversity in mobile communications," *IEEE Trans. Veh. Technol.*, vol. 39, no. 3, pp. 177–185, Jun. 1990.

[2] V. Erceg, P. Soma, D. Baum, and S. Catreux, "Multiple-input multiple-output fixed wireless radio channel measurements and modeling using dual-polarized antennas at 2.5 GHz," *IEEE Trans. Wireless Commun.*, vol. 3, no. 6, pp. 2288 – 2298, Nov. 2004.

[3] M. Shafi, M. Zhang, A. Moustakas, P. Smith, A. Molisch, F. Tufvesson, and S. Simon, "Polarized MIMO channels in 3-D: Models, measurements, and mutual information," *IEEE J. Sel. Areas Commun.*, vol. 24, no. 3, pp. 514–527, Mar. 2006.

[4] S.-C. Kwon, "Geometrical theory, modeling and applications of channel polarization," *Ph.D. Thesis, Georgia Institute of Technology*, pp. 1–128, 2014.

[5] S.-C. Kwon and G. L. Stüber, "Geometrical theory of channel depolarization," *IEEE Trans. Veh. Technol.*, vol. 60, no. 8, pp. 3542–3556, Oct. 2011.

[6] S.-C. Kwon, G. Stüber, A. López, and J. Papapolymerou, "Geometrically based statistical model for polarized body-area-network channels," *IEEE Trans. Veh. Technol.*, vol. 62, no. 8, pp. 3518–3530, Oct. 2013.

[7] D. Landon and C. Furse, "Recovering handset diversity and MIMO capacity with polarization-agile antennas," *IEEE Trans. Antennas Propag.*, vol. 55, no. 11, pp. 3333–3340, Nov 2007.
[8] O. Karabey, S. Bildik, S. Bausch, S. Strunck, A. Gaebler, and R. Jakoby, "Continuously polarization agile antenna by using liquid crystal-based tunable variable delay lines," *IEEE Trans. Antennas Propag.*, vol. 61, no. 1, pp. 70–76, Jan 2013.
[9] S. C. Kwon and A. F. Molisch, "Capacity maximization with polarization-agile antennas in the MIMO communication system," *Proc. IEEE Global Telecommun. Conf.*, pp. 1–6, Dec. 2015.
[10] D. Tse and P. Viswanath, *Fundamentals of Wireless Communication*, 1st ed. Cambridge, 2005.
[11] G. Strang, *Linear Algebra and Its Applications*, 4th ed. Thomson Learning, Inc., 2005.